Hindawi
Advances in Materials Science and Engineering
Volume 2019, Article ID 9504198, 15 pages
https://doi.org/10.1155/2019/9504198

Research Article

Synthesis of Mesoporous TiO_2 Spheres via the Solvothermal Process and Its Application in the Development of DSSC

S. Velázquez-Martínez,[1] **S. Silva-Martínez**,[2] **A. E. Jiménez-González**,[3] **and A. Maldonado Álvarez**[4]

[1]*Posgrado en Ingeniería y Ciencias Aplicadas, Universidad Autónoma del Estado de Morelos, Av. Universidad 1001, Col. Chamilpa, Cuernavaca, Morelos C.P. 62209, Mexico*
[2]*Centro de Investigación en Ingeniería y Ciencias Aplicadas, Universidad Autónoma del Estado de Morelos, Av. Universidad 1001, Col. Chamilpa, Cuernavaca, Morelos C.P. 62209, Mexico*
[3]*Instituto de Energías Renovables, IER-UNAM, Temixco, Morelos C.P. 62580, Mexico*
[4]*CINVESTAV–IPN, Departamento de Ingeniería Eléctrica-SEES, Av. Instituto Politécnico Nacional 2508, Ciudad de México C.P. 07360, Mexico*

Correspondence should be addressed to A. E. Jiménez-González; ajg@ier.unam.mx

Received 12 April 2019; Accepted 1 July 2019; Published 2 September 2019

Guest Editor: Pradip Basnet

This study examined the synthesis of the *n*-type nanostructured titanium dioxide semiconductor using a combined sol-gel/solvothermal method at 200°C, varying the concentrations of H_2O and HCl used as a catalyst for the hydrolysis of the titanium isopropoxide precursor. A white powder of TiO_2 nanoparticles was obtained via the solvothermal process. Scanning electron microscopy revealed a spherical morphology of the TiO_2 nanoparticles, with their diameter ranging from 2 to 7 microns as the HCl concentration increases. High-resolution electron microscopy and X-ray diffraction showed that the spheres are mesoporous titanium oxide ($TiO_2{}^m$) composed of nanocrystals with an anatase crystalline phase whose crystallite diameter grows from 8 to 13 nm as the HCl concentration increases. On the contrary, optimizing the H_2O concentration enabled a decrease in the crystallite size of $TiO_2{}^m$ and increases in the surface area and the energy band gap of $TiO_2{}^m$. The enlarged surface area enabled an increase in the number of contact points between $TiO_2{}^m$ and the dye of dye-sensitized solar cells (DSSCs), resulting in a better solar cell performance. The white powder was used to prepare a $TiO_2{}^m$ film via the screen-printing technique, which was used in the development of DSSC. The performance parameters of the DSSC (I_{SC}, V_{OC}, FF, and η%) were correlated with the synthesis parameters of $TiO_2{}^m$. This correlation showed that H_2O and HCl greatly influence the semiconductor properties of $TiO_2{}^m$, along with the short-circuit current J_{SC} and the conversion efficiency η% of the DSSC.

1. Introduction

Dye-sensitized solar cells (DSSCs) were developed at the beginning of the 90s [1], and today, they represent a mature technology with high marketing potential due to their acceptable stability, high performance under different lighting conditions, relatively low cost of production, and low toxicity [2–4]. The principle of operation of these cells is based on the separation of electrical charge by the junction between semiconductor materials with different electrical conductivities [5]. The active electrode of a DSSC uses an *n*-type mesoporous oxide semiconductor with a large surface area as its main component—in most cases, titanium oxide (TiO_2)—whose crystalline anatase phase is most often used [6–11].

A DSSC has a structure of the type SnO_2 : $F/TiO_2{}^c/TiO_2{}^m/N719/I^-/I_3{}^-/Pt/SnO_2$: F, where SnO_2 : F represents a transparent conductor of high electrical conductivity and optical transmittance, $TiO_2{}^c$ is a thin layer of TiO_2 called the compact layer, $TiO_2{}^m$ is a mesoporous *n*-type semiconductor layer, N719 is a ruthenium dye, $I^-/I_3{}^-$ is the redox pair, and Pt/SnO_2 : F represents a platinum counter electrode deposited on the transparent conductor SnO_2 : F.

During the preparation of the DSSC, the TiO_2^m layer is sensitized with a dye (e.g., N719, N3, or organic dyes) to absorb electromagnetic radiation from the sun.

During the electromagnetic excitation from the HOMO (highest occupied molecular orbital) level to the LUMO (lowest unoccupied molecular orbital) level of the N719 dye, an electron is created at the LUMO level and a hole is formed at the HOMO level. From the LUMO level, the electron is rapidly injected into the conduction band of TiO_2^m and transferred to $SnO_2:F$ through TiO_2^c for subsequent extraction to an external circuit connected to the DSSC [3, 12–15]. To regenerate the ionized HOMO level, it is necessary to transfer an electron to that state from the redox pair (for example, I^-/I^{3-} or Co^{2+}/Co^{3+}), which donates electrons to restore the original state of the dye [3]. To regenerate the redox pair I^-/I^{3-}, the $Pt/SnO_2:F$ counter electrode consisting of a thin layer of platinum functioning as a catalyst is used to facilitate electron collection [16]. Once the photogenerated electrons are injected into the conduction band of TiO_2^m, they are quickly transported to the external circuit, producing an electric current based on a test charge and arriving at the $Pt/SnO_2:F$ counter electrode. Finally, to complete the cycle, the electrons collected in the counter electrode are ready to start a new regeneration cycle of the redox pair [3, 17].

The efficiency of a DSSC depends on the individual performance of each component layer [18, 19]. The semiconductor properties of TiO_2^m are essential in determining the performance of the DSSC. However, these properties depend to a large extent on solid state properties, such as the crystalline phase, crystallite size, porosity, surface area, surface morphology, and electrical conductivity, which depend on the chemical reaction occurring during TiO_2^m synthesis [20]. The crystalline anatase phase of TiO_2^m is one of the most often used phases in preparing DSSC because it allows relatively high conversion efficiencies to be obtained [21–23].

The solvothermal method has widely been used in the synthesis of the nanoparticles of semiconductor materials [24–28]. If water is used as a solvent, the method is known as "hydrothermal synthesis," whereas if some alcohol is used, the process is known as "solvothermal synthesis." Both processes are used to prepare various semiconductor materials of different geometries, such as micro- and nanostructured powders. In addition, it is possible to control the morphology (sphere (3D), rod (2D), or wire (1D)) of the crystals formed via solvent supersaturation, the chemical concentration of the reagents used, and kinetic control [29].

TiO_2^m has a relatively large surface area, allowing greater dye and photon adsorption. Among the different mesoporous nanostructured materials, the synthesis of TiO_2^m spheres—TiO_2^m nanocrystals brought together into spherical assemblies—having a larger surface area than some nanotube and nanowire systems has been demonstrated [30].

Several methods for preparing TiO_2^m spheres using different variations of the solvothermal method have been published in the literature. A characteristic of these synthesis methods is that mesoporous spheres are formed in two steps: (a) formation of TiO_2^m spheres during a sol-gel process and (b) subjection of these spheres to a solvothermal process in an autoclave at temperatures between 150 and 200°C [31–35]. For example, some authors synthesized TiO_2^m precursor spheres from a sol-gel solution in the presence of hexadecylamine, then dried them in the air, and finally subjected them to solvothermal treatment in a mixture of water and ethanol [31, 32]. Another method used to form titania (anatase-rutile) spheres is to add titanium tetraisopropoxide to ethylene glycol to form a white suspension, drying it at 80°C for 10 h. The spheres obtained using this method are dispersed in water and ethanol, placed in an autoclave, and thermally treated at 150°C for 12 h [33]. Another synthesis method of TiO_2^m microspheres is the thermal hydrolysis of titanium sulfate, dissolving it later in *n*-propanol and water, and then performing the solvothermal reaction [34]. The synthesis of TiO_2^m microspheres starting from titanium isopropoxide mixed with anhydrous acetone at ambient conditions is also possible by subjecting the mixture to a solvothermal process at 200°C for 12 h [35].

In the present study, the synthesis of TiO_2^m spheres is performed via a sol-gel/solvothermal process, in which the structural, morphological, optical, and electrical properties of the spheres are essentially studied according to the concentration of hydrochloric acid (as a catalyst for the hydrolysis of the titanium isopropoxide precursor), the H_2O content, and the temperature during the synthesis. Specifically, the surface area of TiO_2^m, pore size distribution, crystallite size, and forbidden energy band gap E_g are studied. This study also examines the application of TiO_2^m in the development of DSSC and the performance parameters (short-circuit current I_{SC}, open-circuit voltage V_{OC}, fill factor FF, and conversion efficiency η%) as a function of the synthesis parameters of the *n*-type TiO_2^m semiconductor.

2. Experimental Section

2.1. Chemical Reagents. To prepare the different component layers of the DSSC, the following reagents and materials were used.

Titanium isopropoxide (Sigma-Aldrich), ethyl alcohol absolute (Fermont), acetone absolute (Fermont), hydrochloric acid (J. T Baker 36.6–38%), and deionized water (Milli®85-Q/RIO) were used. $SnO_2:F$ (FTO) of 15 and 8 ohm per square (TEC15 Pilkington group), terpineol (mixture of isomers anhydrous, Sigma-Aldrich), ethyl cellulose (Sigma-Aldrich), ruthenium dye N719 (Ruthenizer 535-bis TBA Solaronix), polymer Surlyn® (Meltonix 1170-60 Solaronix), and Platinum Paste-PT-1 (Dyesol) electrolyte (Iodolyte HI-30) were also used.

2.2. Deposition of DSSC Films and Cell Assembly

2.2.1. TiO_2^c Layer. To prepare the thin film called the TiO_2^c blocking layer, a mixture of 2.0 mL of deionized water (H_2O) with 93.5 mL of ethanol was stirred in a two-neck flat-bottomed flask, adding 1.5 mL of hydrochloric acid (HCl) as a catalyst for the hydrolysis of the titanium isopropoxide precursor $Ti[OCH(CH_3)_2]_4$ ($Ti(OC_3H_7)_4$) [36–38]. After 20 minutes of stirring, 3 mL of titanium isopropoxide was

added dropwise to the above solution, which was then stirred for 24 h. During the said addition, the titanium precursor is hydrolyzed, forming a sol, to later form the polymer chains of the fully hydrolyzed $Ti(OH)_4$ monomer and thereby form the gel [39]. Using dip coating equipment, 3 depositions are performed on a transparent conductive glass substrate of SnO_2 : F (FTO) with resistivity 15 Ω/□. Subsequently, the substrate is calcined in air at 450°C, where the metal hydroxide is transformed into a titanium oxide film with a thickness of approximately 200 nm. In this way, a SnO_2 : $F/TiO_2{}^c$ junction is obtained.

2.2.2. Synthesis of $TiO_2{}^m$ Nanoparticles via a Sol-Gel/Solvothermal Method

(1) Sol-Gel Process. To prepare $TiO_2{}^m$ nanoparticles, a mixture of 1.9 mL of deionized water (H_2O) with 115.5 mL of ethanol was stirred in a two-neck flat-bottomed flask, adding hydrochloric acid (HCl) as a catalyst for the hydrolysis [36–38]. The volume of HCl was adjusted to obtain 0.5, 1, 1.5, 2, 2.5, and 3% (v/v) concentrations in relation to the total solution volume. After 20 minutes of stirring, 20.73 mL of titanium isopropoxide was added dropwise to the above solution, which was then stirred for 24 h.

(2) Solvothermal Process. After the sol-gel process, the solution was placed in an autoclave and thermally treated for 12 h at 200°C and a pressure of 54 atm. Then, the autoclave was allowed to cool to room temperature, and the solution resulting from the solvothermal process was centrifuged at 4000 rpm for 20 min. Subsequently, the obtained nanoparticles were washed in anhydrous ethanol and then centrifuged at 7000 rpm. This washing process was repeated twice more.

2.2.3. Preparation of the $TiO_2{}^m$ Layer. Using the $TiO_2{}^m$ nanoparticles obtained via the solvothermal method explained in the previous section, a paste was prepared with 0.5 g of $TiO_2{}^m$ mixed with 4.0 g of terpineol as a dispersing agent and 2 mL of acetone; this paste was placed in an ultrasound bath for 1 h to avoid nanoparticle agglomeration and lump formation. In another container, 0.15 grams of ethyl cellulose were weighed and mixed with 8 mL of ethanol, and the mixture was also placed in an ultrasound bath for 1 h. Subsequently, both solutions were mixed, and the ethanol was extracted using a rotary evaporator. The remaining paste was deposited using the screen-printing technique on the SnO_2 : $F/TiO_2{}^c$ junction to obtain a SnO_2 : $F/TiO_2{}^c/TiO_2{}^m$ heterojunction with an area of $0.5 \times 1.0\ cm^2$, which was thermally treated at 530°C for 1 h. Ethyl cellulose was added to create pores in the $TiO_2{}^m$ layer during the thermal treatment.

2.2.4. N-719 Dye. Sensitization of $TiO_2{}^m$ at the SnO_2 : $F/TiO_2{}^c/TiO_2{}^c/TiO_2{}^m$ heterojunction was performed by immersion for 24 h in a 0.5 mM solution of N-719 ruthenium dye in ethanol, which is based on ruthenium-bipyridyl complexes. The N-719 ruthenium dye from Solaronix has the following molecular structure: $C_{58}H_{86}O_8N_8S_2Ru$. To sensitize the *n*-type $TiO_2{}^m$ semiconductor, the dye needs to have the capacity to adhere strongly to the surface of $TiO_2{}^m$, which is achieved through the carboxylic groups of the N-719 dye. The sensitized SnO_2 : $F/TiO_2{}^c/TiO_2{}^m$/dye heterojunction is known as the working electrode because a DSSC constitutes a photoelectrochemical cell.

2.2.5. $I^-/I_3{}^-$ Redox Pair. An electrolyte in a liquid state is a fluid containing ions carrying electric charges. The I^-/I^{3-} redox pair was used in this project and is commonly used for these types of cells [40]. To prepare the electrolyte, solutions of lithium salts (lithium iodide), iodine, and 4-tert-butylpyridine dissolved in acetonitrile are usually mixed. The electrolytic solution (lodolyte HI-30 from Solaronix) is placed in the solar cell to regenerate the dye after it has provided an electron to the $TiO_2{}^m$ conduction band; thus, the electrolyte is the medium allowing the oxidized dye to regenerate and, under electromagnetic excitation, continue injecting electrons into the semiconductor.

2.2.6. Counter Electrode. A platinum film is deposited on SnO_2 : F to generate the Pt/SnO_2 : F counter electrode of the solar cell, considering that Pt is used to expedite electrolyte regeneration. Using the screen-printing technique, a platinum paste (Platinum Paste-PT-1 from Dyesol) was applied on SnO_2 : F, allowed to dry for 30 min at room temperature and then thermally treated at 450°C for 1 h.

2.2.7. DSSC Assembly. To assemble the solar cells studied here, the working electrode was placed with the dye facing up; a spacer (Surlyn® Polymer) was placed with a tweezer to avoid electrical contact between the $TiO_2{}^m$ layer and the counter electrode. Previously, Surlyn® was cut in the form of a frame to cover the area around the $TiO_2{}^m$ layer (1.2 cm × 0.7 cm). Then, the counter electrode was placed on the working electrode so that Surlyn was sandwiched between the glasses as shown in Figure 1.

This arrangement was introduced into a muffle furnace at 215°C for 90 s, then removed from the furnace, and allowed to cool at room temperature for 5 min. Subsequently, the electrolytic solution was injected into the cell through a pair of holes previously drilled in the counter electrode. Finally, silver paint was placed on the ends of the cell for better conductivity in measuring its parameters.

2.3. Experimental Equipment. To study the crystalline phase and crystallite size of the *n*-type $TiO_2{}^m$ semiconductor prepared in this study, we used a Rigaku X-ray diffractometer DMAX-2200, which uses the K_α line ($E = 1.5405$ Å) of a copper anode. The crystallite size of $TiO_2{}^m$ was determined using the Scherrer equation:

$$D = \frac{0.94\lambda}{B\cos\theta}, \quad (1)$$

where λ is the X-ray wavelength, B (2θ) is the full-width at half-maximum intensity (FWHM), and θ is the diffraction

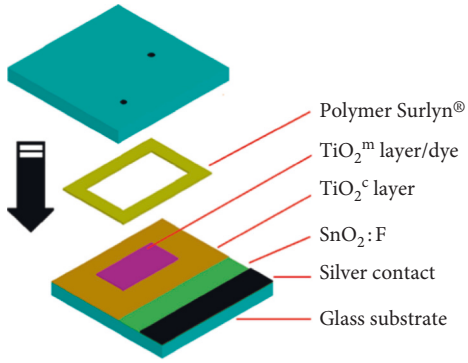

Figure 1: Cell assembly using a Surlyn polymer.

angle. To study the surface morphology of TiO_2^m, micrographs were obtained by field emission scanning electron microscopy (FE-SEM Hitachi S-5500). Reflectance and optical transmittance analyses were performed with a SHIMADZU UV-3101 spectrophotometer. These analyses were then used to calculate the size of the forbidden energy band gap E_g [41]. For the measurement of the I-V curves, a Keithley 236 Source-Measure Unit coupled with the SLB-150A Compact Solar Simulator Class AAA from SCIENCETECH and equipped with a UXL-150S0 Xenon short-arc lamp and an AM Air Mass Filter, was used. The specific surface area (SSA) was calculated using the BET method on a Quantachrome Autosorb 1. Before nitrogen adsorption, the oven-dried and dispersed sample was placed on a Quantachrome 9 mm cell and outgassed at 100°C for 24 h to remove any adsorbed water after storage and transport of the sample. Nitrogen adsorption isotherms were programmed with a 44 data point collection, of which the first 11 were used for SSA calculations.

3. Results and Discussion

3.1. Influence of HCl as a Catalyst for Hydrolysis on the Synthesis of TiO_2^m Nanoparticles. During the synthesis of TiO_2^m nanoparticles via the solvothermal method, the volume of HCl (experimental parameter) as a catalyst for hydrolysis was varied in relation to the total solution volume (% (v/v)) according to the following values: 0.5, 1.0, 1.5, 2.0, 2.5, and 3.0% (v/v). The H_2O concentration was fixed during this process at 1.9% (v/v). The TiO_2^m nanoparticles prepared using this method were characterized by X-ray diffraction and FE-SEM. This experiment showed that HCl, as a catalyst for the hydrolysis of titanium isopropoxide, plays a fundamental role in the properties of TiO_2^m nanoparticles synthesized during the sol-gel/solvothermal process as described below.

3.1.1. TiO_2^m Nanoparticles Prepared via the Solvothermal Process at 200°C. Figure 2 shows the X-ray diffraction patterns of TiO_2^m for each HCl concentration used (0.5 to 3.0% (v/v)) during the solvothermal processes at 200°C. A dominant peak at an angle of $2\theta = 26.1°$ corresponding to the (101) plane of the pure anatase crystalline phase—according to the *Powder Diffraction File* database card # 21-1272—and

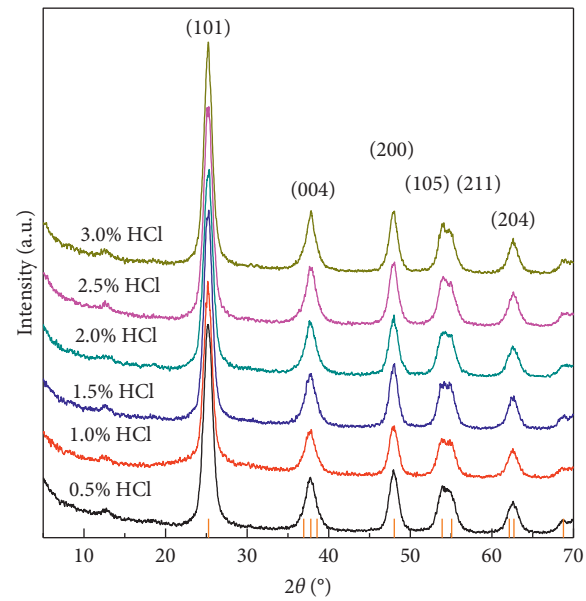

Figure 2: X-ray diffraction patterns of TiO_2^m nanoparticles prepared at 200°C in an autoclave as a function of HCl concentration.

other reflections corresponding to its other crystalline planes are observed. Relatively wide peaks corresponding to relatively small crystallite sizes (8–12 nm), as discussed below, are observed.

3.1.2. Thermal Treatment of TiO_2^m Nanoparticles in Air at 530°C. As explained in Section 2.2.3, a paste was made with TiO_2^m nanoparticles prepared using the solvothermal process for the deposition of the mesoporous layer via the screen-printing technique on the SnO_2 : F/TiO_2^c junction to obtain the SnO_2 : F/TiO_2^c/TiO_2^m heterojunction, which was thermally treated in air at 530°C for 3 h. After thermal treatment, an X-ray diffraction study was performed on each sample listed in Figure 2, with the results shown in the graph of Figure 3. This graph shows that the anatase crystalline phase is conserved for all HCl concentrations, except for 2.5 and 3.0% (v/v) HCl concentrations, where a small peak can be perceived (R) at an angle of $2\theta = 27.2°$, corresponding to the rutile crystalline phase. With thermal treatment, diffraction peaks are sharper, so the crystallite size has increased (17 to 22 nm), as reported in Table 1.

3.1.3. FE-SEM of TiO_2^m Prepared at Different HCl Concentrations. Figure 4 shows micrographs of the surface morphology of TiO_2^m taken with the FE-SEM S-5500 microscope (10,000X) for each HCl concentration used during the sol-gel/solvothermal process at 200°C. These micrographs show how the HCl concentration significantly influences the morphology of TiO_2^m particles, which changes from a relatively smooth surface, as observed in Figures 4(a) and 4(b), corresponding to the synthesis of TiO_2^m at 0.5 and 1.0% (v/v) HCl concentrations, respectively, to one in which agglomeration of TiO_2^m particles begins, as shown in Figure 4(c), corresponding to a 1.5% (v/v) HCl concentration. Figure 4(d)

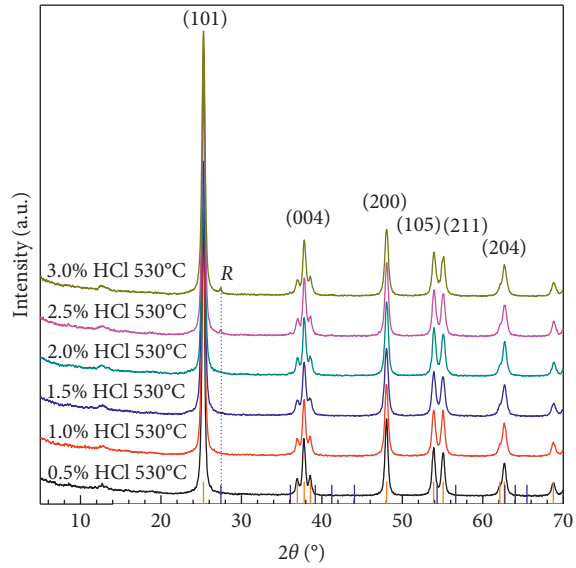

Figure 3: X-ray diffraction patterns of $TiO_2{}^m$ nanoparticles prepared at 530°C as a function of HCl concentration.

Table 1: Crystallite diameter, pore size, surface area, and band gap E_g of $TiO_2{}^m$ samples prepared in an autoclave at 200°C and at 530°C.

HCl% (v/v)	Crystallite size (nm)	Pore size (nm)	Surface area (m^2/g)	Crystallite size (nm)	Pore size (nm)	Surface area (m^2/g)	E_g (eV)
	200°C			530°C			
0.5	8.45	2.96	161.10	22.20	10.72	31.75	3.18
1.0	9.93	4.21	196.00	19.90	12.35	47.30	3.23
1.5	11.54	15.12	183.90	17.60	41.11	65.56	3.27
2.0	11.50	6.57	208.70	20.00	23.56	55.46	3.31
2.5	11.75	5.96	208.10	19.30	19.75	56.83	3.25
3.0	12.05	6.43	198.50	18.40	16.83	60.12	3.32

shows a semispherical morphology corresponding to the 2.0% (v/v) HCl concentration, where a clear coalescence is observed as larger spheres grow from the fusion with smaller spheres of $TiO_2{}^m$. As the HCl concentration increases to 2.5 and 3.0% (v/v), more perfect and larger $TiO_2{}^m$ spheres with diameters above 6 microns are obtained (Figure 4(e)), and Figure 4(f) shows even larger $TiO_2{}^m$ spheres with irregular agglomerates beginning to grow on their surfaces. Notably, Kim et al. [42] also reported the synthesis of $TiO_2{}^m$ spheres in acid media (a mixture of H_2SO_4 and HNO_3) using surfactants as nucleation precursors during the sol-gel process and a subsequent hydrothermal treatment to obtain highly spherical morphologies such as those shown in this study.

Figures 5 and 6 show images of the $TiO_2{}^m$ samples included in Figure 4 at a 300,000X and 500,000X magnification, respectively, where each sample, including the spheres, are made of $TiO_2{}^m$ nanocrystals. Figures 5 and 6 show that all samples have pores and that the pore diameter grows from 10 to 23 nm when the HCl concentration increases from 0.5 to 3.0% (v/v).

The magnification increase from 300,000X to 500,000X allowed us to observe in a much better form the surface morphology as well as the pore size distribution of $TiO_2{}^m$ synthesized at different HCl concentrations. For example, from Figures 4(a)–4(d), it is easy to see a pore size increase as the HCl concentration varies from 0.5 to 2.0% (v/v), and after that, the pore size remains almost constant. Also, the crystal size can be much better estimated, as shown in Figure 6, and its value coincides with the determined by X-ray diffraction (8–12 nm), as explained in Section 3.1.1.

3.1.4. Surface Area, Crystallite Size, Pore Size, and E_g of $TiO_2{}^m$ as a Function of HCl Concentration. The crystallite size, surface area, and pore size play a fundamental role in the performance of DSSC. For example, the smaller the crystallite size is, the larger the surface area will be, which allows us to have many *p-n* junctions between the dye and $TiO_2{}^m$. Table 1 shows the average crystallite diameter, pore size, and surface area of $TiO_2{}^m$ samples in powder form after their synthesis in the autoclave at 200°C for each HCl concentration used. To use it in the development of DSSC, $TiO_2{}^m$ must be subjected to thermal treatment in air at 530°C. Table 1 also shows the values of the average crystallite diameter, pore size, surface area, and band gap of $TiO_2{}^m$ powders treated at 530°C for 3 h.

Considering only the pore size obtained for the titanium dioxide samples treated at 200 and 530°C, it is possible to conclude from Table 1 that the material is mesoporous, according to the IUPAC definition [43] because, for all cases, the pore size of $TiO_2{}^m$ remains below 50 nm.

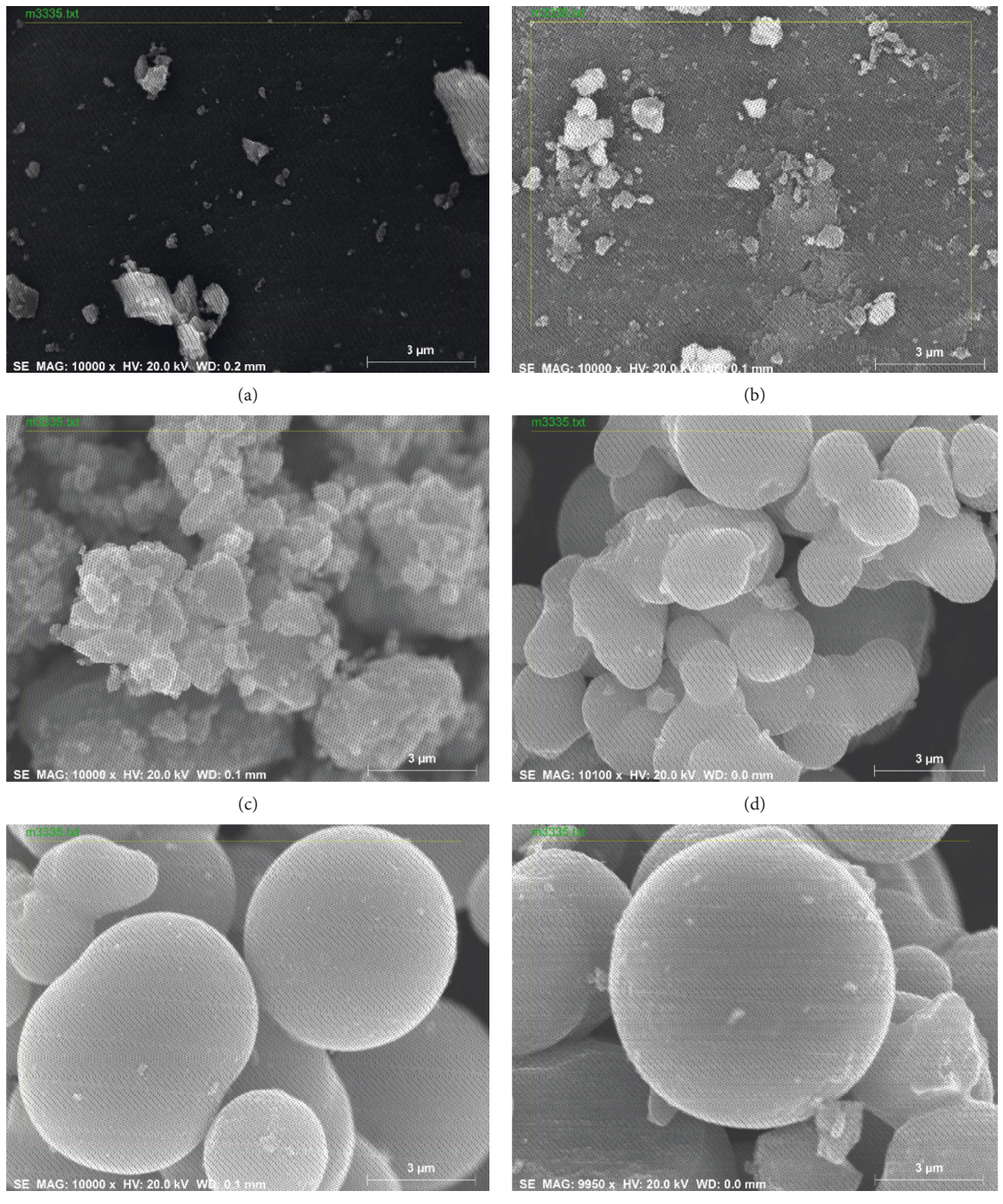

Figure 4: Micrographs of TiO_2^m (10,000X magnification) synthesized at different HCl concentrations: (a) 0.5, (b) 1.0, (c) 1.5, (d) 2.0, (e) 2.5%, and (f) 3.0% (v/v).

Considering the results of Table 1, columns 4 and 7 show the surface area of TiO_2^m as a function of HCl concentration for samples treated at 200°C (solvothermal process) and at 530°C, respectively. The surface area decreases drastically from an average of 198 to 52 m^2/g as the temperature changes from 200 to 500°C. This decrease in surface area is due to crystallite size growth (diameter), as observed from columns 2 and 5, and to particle coalescence into spherical configurations to form larger TiO_2^m spheres, favoring the increase in pore size observed in columns 2 and 6 of Table 2.

Columns 3 and 6 show a maximum pore size of 15.12 nm at 200°C and 41.11 nm at 530°C, both at 1.5% (v/v) HCl concentration. The pore size decreases above the 1.5% (v/v) HCl concentration. This decrease can be attributed to a competition between the decrease in crystallite size from 20.0 to 18.4 nm shown in Table 1 and the formation of larger TiO_2^m spheres as the HCl concentration increases above 1.5% (v/v).

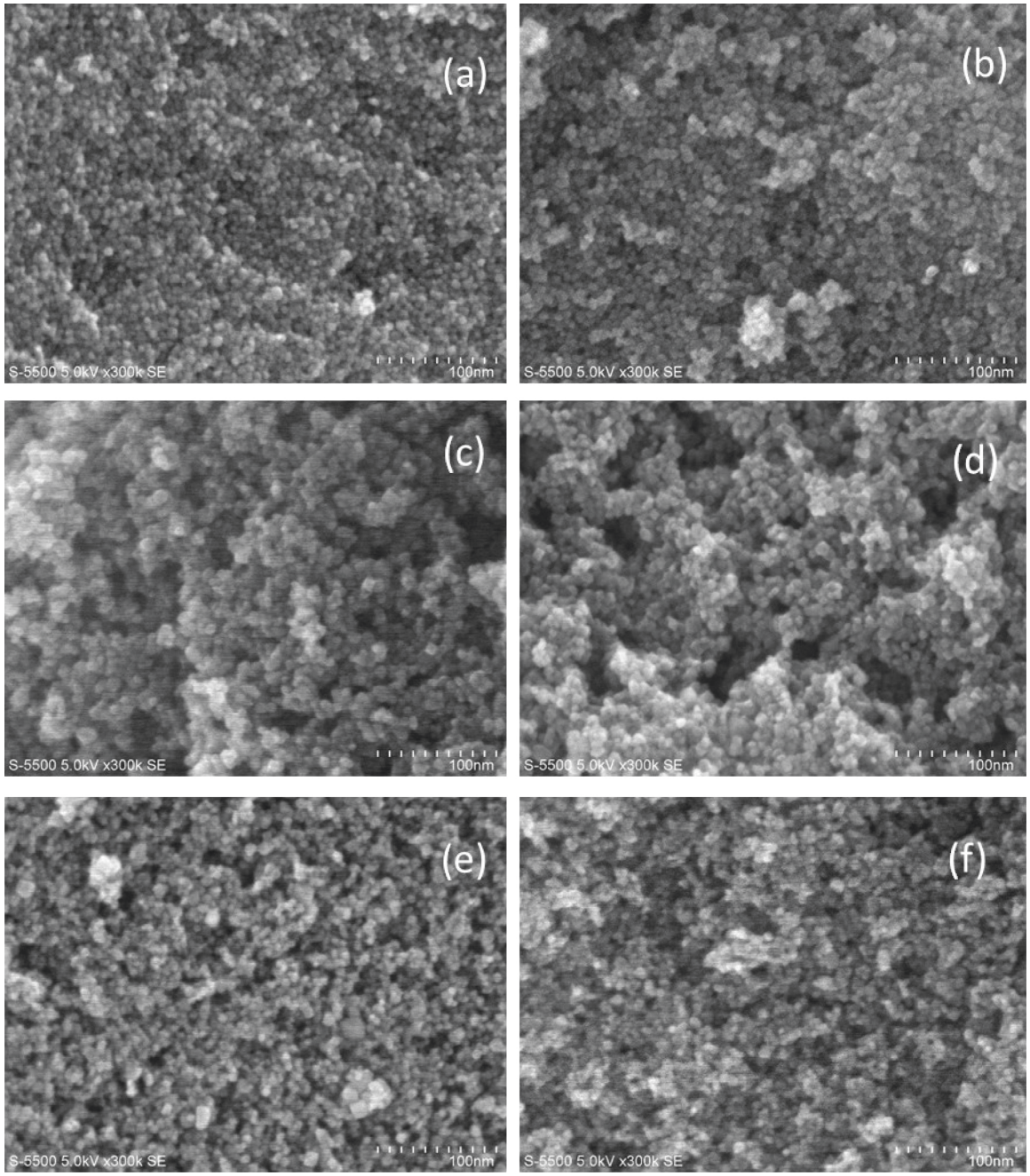

Figure 5: Micrographs (300,000X magnification) of $TiO_2{}^m$ synthesized at different HCl concentrations: (a) 0.5, (b) 1.0, (c) 1.5, (d) 2.0, (e) 2.5, and (f) 3.0% v/v.

3.2. Influence of H_2O during Hydrolysis on the Synthesis of $TiO_2{}^m$ Nanoparticles

3.2.1. $TiO_2{}^m$ Samples Obtained at Different H_2O Concentrations. Once the effect of HCl concentration on preparing $TiO_2{}^m$ via the solvothermal process was studied, the role of the H_2O content during the synthesis of $TiO_2{}^m$ was analyzed. To this end, X-ray diffraction studies were performed on the $TiO_2{}^m$ films prepared via the solvothermal process at 200°C, taking the 2.5% (v/v) HCl concentration as a fixed experimental parameter and varying the H_2O concentration from 1.9 to 4.9% (v/v). All cases show an X-ray diffraction pattern of the $TiO_2{}^m$ anatase crystalline phase very similar to that in Figure 2. It was also observed that for the 3.9% (v/v) H_2O concentration, there are small indications of the growth of a brookite phase at an angle of $2\theta = 30.8^\circ$ corresponding to the (121) plane.

3.2.2. $TiO_2{}^m$ Samples Treated at 530°C. Because the $TiO_2{}^m$ layer in the development of DSSC was thermally treated in air at 530°C for 3 h, after calcining at that temperature, these samples were subjected to an X-ray diffraction study.

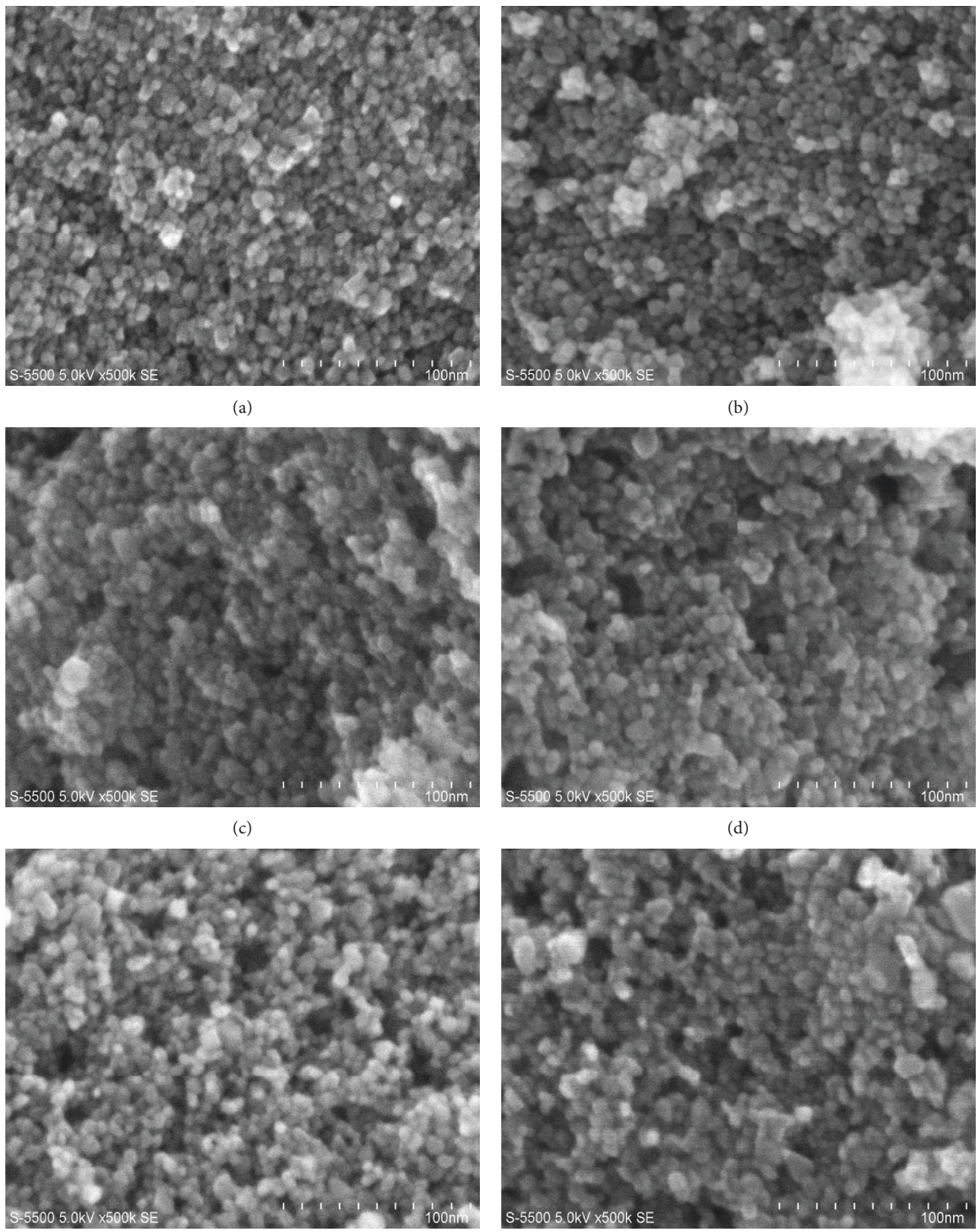

Figure 6: Micrographs (500,000X magnification) of $TiO_2{}^m$ synthesized at different HCl concentrations: (a) 0.5, (b) 1.0, (c) 1.5, (d) 2.0, (e) 2.5, and (f) 3.0% v/v.

The diffraction pattern found in these samples is very similar to that shown in Figure 3 for samples prepared at different HCl concentrations. Here, the anatase crystalline phase is conserved for all H_2O concentrations except for 2.5 and 3.0% (v/v), where a small peak can be perceived at $2\theta = 27.5^{\circ}$C, corresponding to the rutile crystalline phase (R). On the contrary, it is also possible to observe that after said thermal treatment at 530°C, the brookite phase disappears for all H_2O concentrations at which it could be observed.

Table 2: Crystallite diameter, surface area, pore size, and forbidden energy band gap E_g of $TiO_2{}^m$ samples thermally treated in air at 530°C as a function of the H_2O concentration.

H_2O% (v/v) (530°C)	Crystallite size (nm)	Surface area (m^2/g)	Pore size (nm)	E_g (eV)
1.9	19.30	56.83	19.75	3.18
2.4	18.40	56.29	17.19	3.23
2.9	18.10	62.52	33.14	3.27
3.4	16.60	68.15	30.89	3.31
3.9	16.90	71.40	22.93	3.25
4.9	17.10	66.84	22.17	3.32

3.2.3. Analysis of the $TiO_2{}^m$ Surface Area and Pore Size as a Function of H_2O Concentration. For use in the development of DSSC, $TiO_2{}^m$ powders should be thermally treated at 530°C in air for 3 h. Table 2 shows the average crystallite diameter, surface area, and pore size of $TiO_2{}^m$ samples prepared at different H_2O concentrations, maintaining the HCl concentration at 2.6% (v/v) and thermally treated in air at 530°C.

Comparing the columns pertaining to crystallite size in Tables 1 and 2, one finds that for treatment at 530°C, on average (not shown in tables), the $TiO_2{}^m$ crystallite size decreases more with increasing H_2O concentration (17.3 nm) than with increasing HCl concentration (19.56 nm), and consequently, the surface area and forbidden band of $TiO_2{}^m$ should grow slightly with increasing H_2O concentration. Similarly, by comparing the corresponding columns for the pore size shown in Tables 1 and 2, one finds that for treatment at 530°C, on average, a larger $TiO_2{}^m$ pore size is more favored by increasing the concentration of H_2O (24.34 nm) than by increasing that of HCl (20.72 nm).

The findings described in the previous paragraph should be revealed by an increase in the surface area upon optimizing the H_2O concentration. Indeed, by comparing the columns pertaining to the surface area in Tables 1 and 2, one finds that for treatment at 530°C, on average, a larger $TiO_2{}^m$ surface area is more favored by an increase in H_2O concentration (63.97 m^2/g) than by an increase in HCl concentration (52.83 m^2/g). An increasing surface area increases the number of contact points between $TiO_2{}^m$ and the dye, and this is reflected in the solar cell performance as seen later.

3.3. $TiO_2{}^m$ Crystallite Size as a Function of HCl and H_2O Concentrations. Curve (a) in Figure 7 shows the crystallite size of $TiO_2{}^m$ in samples prepared in the autoclave at a temperature of 200°C as a function of HCl concentration, maintaining a fixed 1.9% (v/v) H_2O concentration. As shown in Table 1, the crystallite size increases from 8.45 to 11.04 nm as the HCl concentration increases from 0.5 to 1.5% (v/v); above this last value, the crystallite grows more slowly and reaches a constant value close to 12 nm. This behavior could be due to the hydrolysis of titanium isopropoxide, in which the substitution of the isopropoxy groups $O(C_3H_7)^-$ of titanium isopropoxide by OH^- groups is relatively slow, and as HCl is added, hydrolysis speeds up, causing an increase in crystallite size up to a concentration of 1.5% (v/v), at which the chemical bonds between Ti^{4+} and OH^- hydroxyl radicals reach saturation. Above the 1.5% (v/v) HCl concentration, the crystallite growth is very slow and almost constant. Curve (b) in Figure 7 shows the crystallite sizes of $TiO_2{}^m$ prepared in the autoclave at 200°C by varying the H_2O concentration and taking as a fixed parameter a 2.5% (v/v) HCl concentration. From that curve, it is possible to observe that the crystallite size of the TiO_{2m} semiconductor undergoes a slight decay from 11.8 to 10.6 nm as the H_2O concentration increases from 1.9 to 4.9% (v/v).

3.4. Forbidden Energy Band Gap of $TiO_2{}^m$ as a Function of HCl and H_2O Concentrations. According to the theory of quantum confinement, when the size (diameter) of a crystallite in a crystalline solid decreases to a few nanometers (2–20 nm), the magnitude of the forbidden energy band gap varies. To calculate the forbidden energy band gap E_g, $TiO_2{}^m$ nanoparticles were synthesized at different HCl and H_2O concentrations and thermally treated in air at 530°C. Because $TiO_2{}^m$ has an indirect energy band, a graph of $(\alpha \cdot h\nu)^{1/2}$ vs. $h\nu$ was drawn. In this mathematical expression, α is the absorption coefficient of $TiO_2{}^m$ and is calculated using equation (2), where d is the film thickness, T is the transmittance, and R is the optical reflectance of the material [44]. The tangent line to the curve intersecting the $h\nu$ axis indicates a very approximate value of the forbidden energy band gap:

$$\alpha = \frac{1}{d} * \ln\left(\frac{100 - R}{T}\right). \quad (2)$$

Following the procedure described above, the value of the indirect energy band gap E_g was determined for each HCl concentration used during the synthesis of $TiO_2{}^m$, maintaining a 1.9% (v/v) H_2O concentration as a fixed parameter.

Curve (a) in Figure 8 shows the values of the indirect energy band gap E_g determined for each HCl concentration used for the synthesis of $TiO_2{}^m$. As the HCl concentration increases from 0.5 to 2% (v/v) in the synthesis of the particles, E_g decreases from 3.375 to 3.18 eV; above this concentration, E_g increases slightly until reaching 3.26 eV. These results suggest that optical properties, particularly the absorption coefficient of $TiO_2{}^m$, depend on the synthesis of the material [45].

Curve (b) in Figure 8 shows the magnitude of the indirect forbidden energy band gap E_g of $TiO_2{}^m$ treated at 530°C (HCl concentration = 2.5% (v/v)). This figure shows that the forbidden energy band gap increases from 3.18 to 3.32 eV when the H_2O content varies from 1.9 to 4.9% (v/v). The growth in the magnitude of the forbidden energy band gap is consistent with the decrease in crystallite size from 19.3 to 17.1 nm shown in Table 2, which can be attributed to a quantum confinement effect, as explained by Sánchez et al. [46].

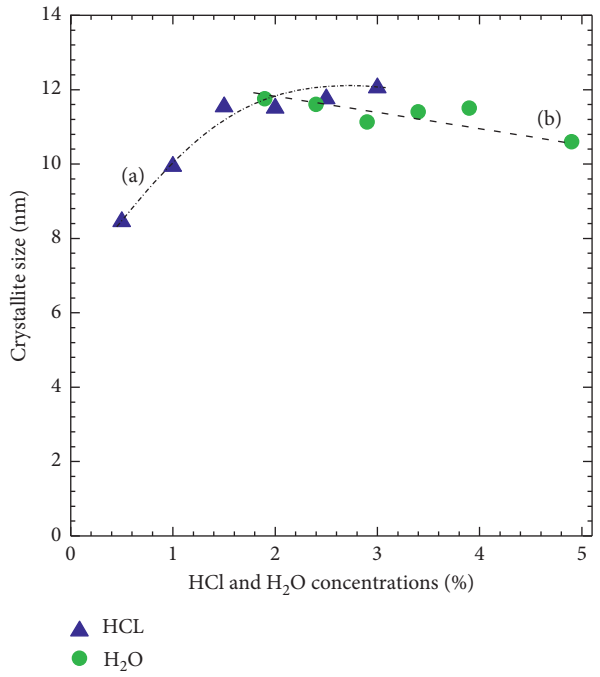

Figure 7: Crystallite size as a function of (a) HCl and (b) H_2O concentrations.

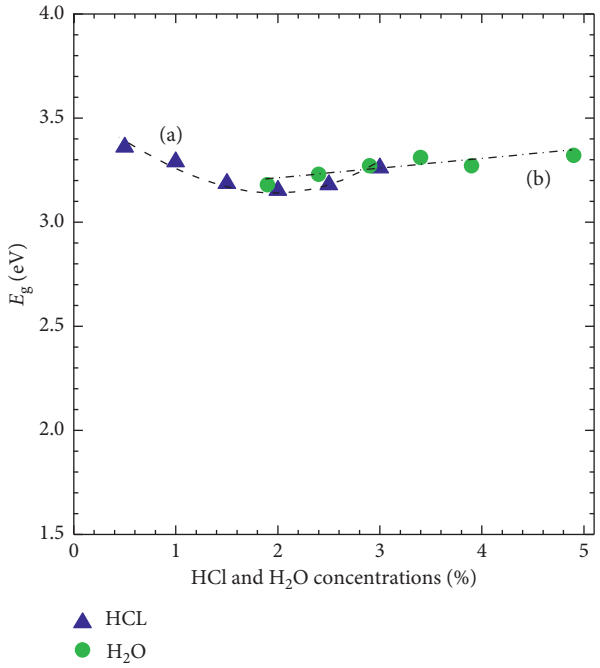

Figure 8: Band gap behavior of TiO_2^m as a function of the (a) HCl and (b) H_2O concentrations after thermal treatment in air at 530°C.

3.5. Photovoltaic Performance Analysis of DSSC

3.5.1. Effect of HCl on the Photovoltaic Performance of DSSC. Once the TiO_2^m semiconductor was prepared, the DSSC was assembled with a structure of the type SnO_2: $F/TiO_2^c/TiO_2^m/N719/I^-/I_3^-/Pt/SnO_2$: F. Here, the TiO_2^m layers were thermally treated in air at 530°C, having a thickness close to 12 microns.

Figure 9 shows the current-voltage curves (I-V) for the different HCl concentrations used in the synthesis of the *n*-type TiO_2^m semiconductor via the solvothermal process. As shown, the HCl concentration drastically influences the performance of the DSSC, where the parameter most influenced is the short-circuit current density J_{SC} and thus the conversion efficiency η% of the solar cell.

The short-circuit current density J_{SC} starts at 4.2 mA/cm^2 for the 0.5% (v/v) HCl concentration and reaches a value of 10.14 mA/cm^2 for the 2.0% (v/v) HCl concentration; above this concentration, J_{SC} decreases to 8.83 mA/cm^2 for the 3.0% (v/v) HCl concentration.

Table 3 summarizes the performance parameters of the DSSC shown in Figures 9 and 10, that is, the open-circuit voltage (V_{OC}), the short-circuit current density (J_{SC}), the fill factor (FF), and the energy conversion efficiency (η%) of the DSSC obtained by varying the concentration of HCl as a catalyst for the hydrolysis of titanium isopropoxide as well as the H_2O content during the sol-gel/solvothermal process.

With the data presented at the left side of Table 3, Figure 10(a) shows a graph of the short-circuit current J_{SC} as a function of the concentration of HCl for the hydrolysis, showing a maximum at J_{SC} = 10.14 mA/cm^2 and 2.0% (v/v) HCl.

The conversion efficiency η% shows a behavior analogous to that of J_{SC}. As shown in Figure 10(b), as the concentration of the HCl hydrolysis catalyst is increased from 0.5 to 2.5% (v/v), η% increases from 2.06% to 3.91%. Above this HCl concentration (2.5% (v/v)), η% decreases to 3.69%.

Table 3 (left side) shows a small variation in the open-circuit voltage V_{OC} upon increasing the concentration of HCl for the hydrolysis from 0.5 to 2.5% (v/v). In this case, the open-circuit voltage V_{OC} decreases slightly from 0.73 to 0.68 V and then increases again to 0.7 V at the 3.0% (v/v) HCl concentration, yielding an average value of V_{OC} = 0.695. Likewise, the fill factor (FF) decreases from 0.68 to 0.52 as the HCl concentration increases from 0.5 to 2.0% (v/v) and then increases again slightly to 0.59 at the 3.0% (v/v) HCl concentration, for an average value of FF = 0.616.

3.5.2. Effect of the H_2O Content on the Photovoltaic Performance of DSSC. Figure 11 shows the I-V curves of DSSC utilizing the TiO_2^m semiconductor prepared with a 2.5% (v/v) HCl concentration for the hydrolysis of titanium isopropoxide and varying H_2O content during the sol-gel/solvothermal process. According to Figure 10(b), 2.5% (v/v) HCl concentration optimizes the efficiency of the DSSCs prepared using the TiO_2^m semiconductor. Table 3 (right side) shows the performance parameters of the DSSC shown in Figure 11: V_{OC}, J_{SC}, FF, and η% of the DSSC obtained by varying the H_2O content.

The right side of Table 3 shows that DSSC prepared from TiO_2^m synthesized at different H_2O contents have more uniform and less disperse values of the open-circuit voltage V_{OC} and fill factor (FF) than the corresponding values found at the left side of Table 3 for TiO_2^m synthesized at different

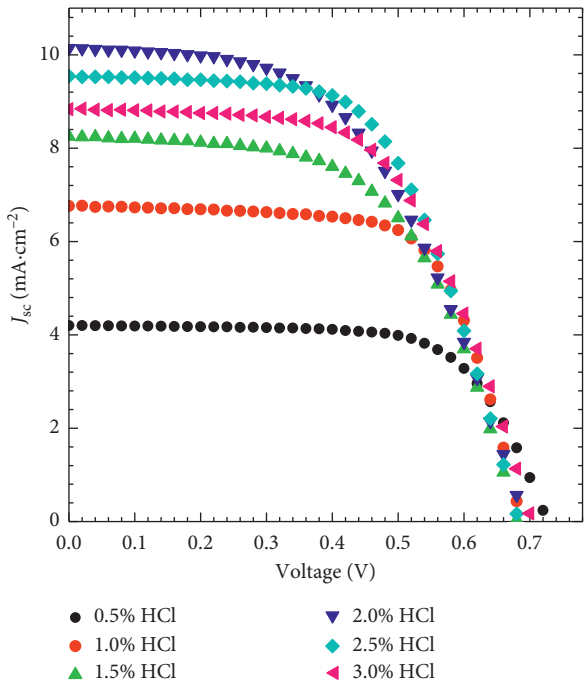

Figure 9: I-V curves of DSSC with *n*-type semiconductors prepared at different concentrations of HCl as a catalyst for the hydrolysis.

Table 3: Performance parameters of solar cells. Left side: DSSCs utilizing TiO_2^m synthesized via a sol-gel/solvothermal process at different HCl concentrations and at a 1.9% (v/v) H_2O concentration and thermally treated in air at 530°C. Right side: DSSCs prepared from TiO_2^m synthesized at different H_2O contents and at a 2.5% (v/v) HCl concentration for the hydrolysis and thermally treated in air at 530°C.

HCl% (v/v)	V_{OC} (V)	J_{SC} (mA·cm^{-2})	FF	η (%)	H_2O% (v/v)	V_{OC} (V)	J_{SC} (mA·cm^{-2})	FF	η (%)
0.5	0.73	4.20	0.68	2.06	1.9	0.68	9.54	0.60	3.91
1.0	0.69	6.76	0.68	3.15	2.4	0.69	9.38	0.63	4.07
1.5	0.68	8.61	0.63	3.65	2.9	0.70	7.27	0.64	3.26
2.0	0.69	10.14	0.52	3.66	3.4	0.69	8.44	0.64	3.69
2.5	0.68	9.54	0.60	3.91	3.9	0.68	9.45	0.63	4.08
3.0	0.70	8.83	0.59	3.69	4.9	0.67	9.16	0.65	3.99

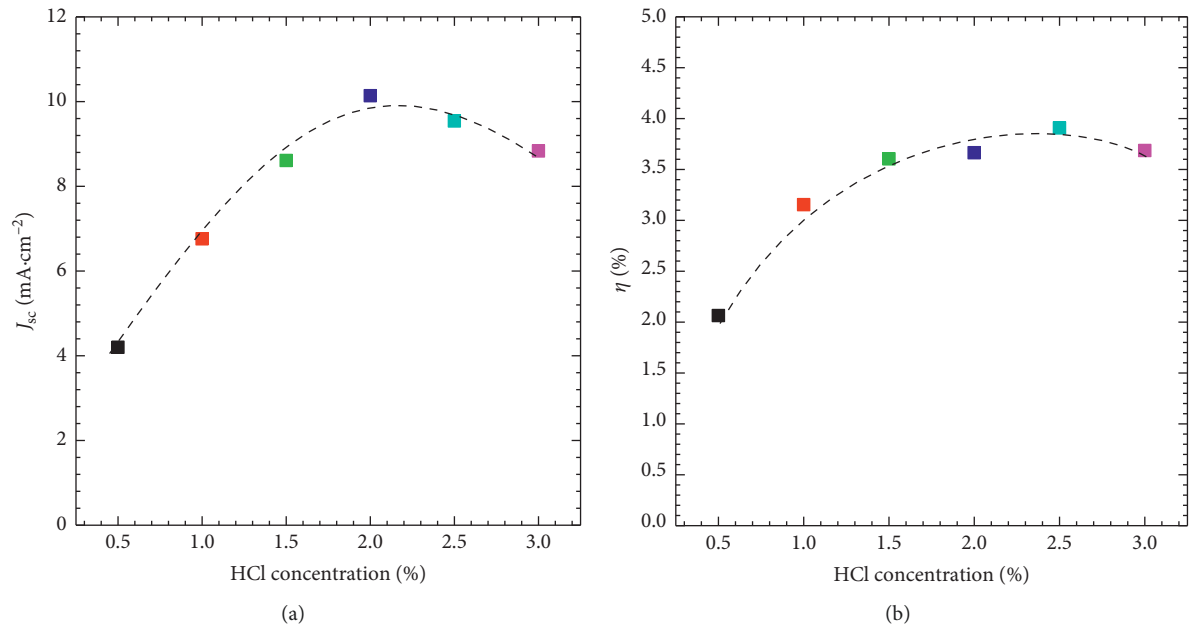

Figure 10: (a) Behavior of the short-circuit current J_{SC} and (b) conversion efficiency as a function of the concentration of HCl for the hydrolysis.

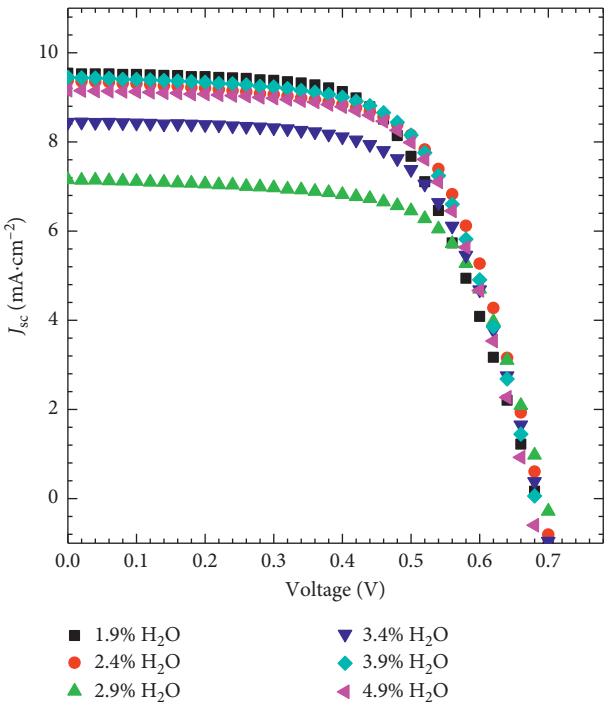

Figure 11: I-V curve of DSSC with n-type semiconductors prepared at different H_2O concentrations and at a 2.5% HCl concentration for the hydrolysis.

HCl concentrations. The open-circuit voltage V_{OC} remains almost constant around its average value of 0.685 V when there is a variation in H_2O content, in contrast to an average value of $V_{OC} = 0.695$ V when there is a variation in HCl concentration. Likewise, the fill factor (FF) remains almost constant around its average value of 0.631 when there is a variation in H_2O content, in contrast to an average value of FF = 0.616 when there is a variation in HCl concentration.

By comparing the average values of the short-circuit currents J_{SC} of the DSSCs in Figures 9 and 11, one finds that the average J_{SC} (H_2O; $J_{SC} = 8.873$ mA/cm^2) of the DSSC in Figure 11 surpasses that in Figure 9 (HCl; $J_{SC} = 8.13$ mA/cm^2), so the average conversion efficiency of the solar cells in Figure 11 ($\eta\% = 3.83\%$) exceeds the average conversion efficiency of the corresponding ones in Figure 9 ($\eta\% = 3.35\%$).

3.6. On the Method of Preparing Mesoporous Spheres and the Conversion Efficiency Achieved. There is a substantial difference between the preparation methods for mesoporous spheres described in the introduction and the one developed in this study. In the previous methods [31–35], the mesoporous spheres are formed in the first step of the sol-gel solution, then extracted, dried, and passed to the solvothermal process in an autoclave. In the present method, $TiO_2{}^m$ microspheres are formed within the autoclave under the influence of a coalescence process at 200°C and HCl, which, with increasing concentration, produces larger mesoporous spheres, as observed in the FE-SEM studies shown in Figure 4.

For comparison purposes of the results obtained in this work, in the literature, it is possible to find other research works related to the synthesis of TiO_2 microspheres with an anatase crystalline phase and its application in dye-sensitized solar cells.

Zhao-Qian and coworkers developed a modified solvothermal process to carry out the synthesis of TiO_2 microspheres using acetone as solvent [35]. As-prepared TiO_2 spheres with diameters from 550 to 1010 nm are composed of densely interconnected nanocrystals with each other and possess a high specific surface area up to 138.47 m$^2\cdot$g^{-1}. As n-type semiconductor integrated in DSSC, Zhao-Qian and coworkers prepared TiO_2 microsphere films via screen printing. With the work electrode (dye-sensitized TiO_2 microspheres), DSSC provided a power conversion efficiency of 7.80%. Finally, TiO_2 microsphere-based DSSCs were optimized by adding a TiO_2 nanocrystal underlayer and $TiCl_4$ post-treatment providing a better performance.

In addition, Swathy et al. prepared anatase titania microspheres by a modified sol-gel method [47]. At first, they took a defined amount of titanium (IV) butoxide (TB) and ethylene glycol, which were mixed and stirred constantly for 24 hours. Subsequently, to the previous solution, they added a water-acetone mixture. The final precipitate was washed, filtered, and dried. The powder obtained, which was further heat treated at 500°C, contained spherical titania particles with a diameter of ~400 nm. The titania microspheres were then used as the scattering layer in DSSC. To assemble DSSCs, Swathy et al. deposited the scattering layer by screen printing on a nanocrystalline titania coating. DSSC with scattering layer achieved photovoltaic parameters, such as V_{oc} of 0.690 V, J_{sc} of 10.44 mA/cm^2, fill factor of 0.68, and a conversion efficiency of 4.92%.

Another work on the preparation of anatase TiO_2 spheres is that reported by Ch. Dwivedia at al. where TiO_2 hollow spheres were synthetized in a continuous spray pyrolysis reactor, using titanium isopropoxide as organic precursor and ethanol as solvent [48]. TiO_2 powder was collected from the outlet of the furnace. This powder was then utilized to make TiO_2 paste using ethanol as solvent. The size of TiO_2 hollow spheres was about 170–300 nm, and the thickness of the shell was about 55–60 nm. TiO_2 hollow spheres were utilized as a scattering layer in dye-sensitized solar cells (DSSCs). Commercial nanocrystalline TiO_2 paste (20 nm) forming the transparent layer was from Dyesol. DSSC containing TiO_2 hollow spheres layer showed a power conversion efficiency of 7.46% which is better than that containing single layer TiO_2 transparent film (7.1%).

Finally, Miao et al. also prepared mesoporous anatase TiO_2 microspheres with different surface areas obtained by a solvothermal process [49]. To do so, tetrabutyl titanate (TBT) was slowly added to an acetone-phenol mixed solvent under vigorous stirring at room temperature. The resulting solution was transferred into a 40 mL Teflon-lined stainless steel autoclave, and then heated at 150°C for 24 h. The samples were then sintered at 500°C. By tuning the ratio of the mixed solvent, the authors obtained high-quality TiO_2 microspheres with controllable surface areas of 122–168 m$^2\cdot$g^{-1}. Then, the mesoporous anatase TiO_2 microspheres were used as the

scattering layer of the photoelectrode. DSSC based on a photoelectrode with a TiO_2 nanoparticle underlayer and a microsphere scattering layer yield the highest photoelectrical conversion efficiency of 7.94%.

In summary, we have seen that TiO_2 microspheres can be synthetized by several preparation methods utilizing different titanium precursors and solvents. TiO_2 microspheres synthetized here (Table 1) or reported in the literature have a large surface area, are mesoporous, and can be used for light scattering in DSSC, allowing for a good charge collection efficiency.

On the contrary, to explain the reason for the relatively low conversion efficiency (4.07%) obtained in the DSSC prepared here, it should be understood that the use of mesoporous spheres in the $TiO_2{}^m$ semiconductor layer has certain disadvantages compared to a compact and homogeneous mesoporous layer (nanoparticle underlayer or nanocrystalline titania coating) of $TiO_2{}^m$: (a) There are gaps between spheres that do not contribute to the formation of the $TiO_2{}^m$/dye junctions. (b) The spherical morphology reduces the surface area, lessening contact between $TiO_2{}^m$ and the dye. (c) The spherical morphology reduces the number of electronic paths for electric current transport after dye excitation. All these facts are detrimental to the conversion efficiency of the DSSC developed here.

To increase the conversion efficiency of the DSSC developed in this study, it would be very convenient to work with the following alternatives in the near future:

(a) Mix $TiO_2{}^m$ spheres with $TiO_2{}^p$ in powder form (called nanoparticle underlayer or nanocrystalline titania coating) without a spherical morphology to fill the gaps between $TiO_2{}^m$ spheres and thus build DSSC.

(b) Use a mesoporous $TiO_2{}^p$ layer in powder form (without a spherical morphology), depositing the mesoporous spheres on that layer, that is, build the solar cell heterostructure with the configuration SnO_2 : $F/TiO_2{}^c/TiO_2{}^p/TiO_2{}^m/N719/I^-/I_3{}^-/Pt/SnO_2 : F$. In the said heterostructure, the $TiO_2{}^m$ layer would function as a scattering layer, as already reported in the literature, which would result in a structure with greater conversion efficiency [50].

4. Conclusions

The structure and morphology of the $TiO_2{}^m$ nanoparticles prepared via a sol-gel/solvothermal method are greatly influenced by the HCl and H_2O concentrations used during hydrolysis of the titanium isopropoxide precursor. HCl greatly changes the morphology of $TiO_2{}^m$ and, as a function of concentration, contributes to obtaining either a planar configuration or a spherical morphology, that is, mesoporous microspheres. On the contrary, optimizing the H_2O concentration enabled a decrease in the crystallite size of $TiO_2{}^m$ and consequently increases in the surface area, pore size, and energy band gap of $TiO_2{}^m$. The increase in surface area allowed the number of contact points between $TiO_2{}^m$ and the dye to increase, which was positively reflected in the solar cell performance. However, in all the synthesis processes performed in this study, it was possible to obtain $TiO_2{}^m$ in a predominantly anatase crystalline phase.

The HCl and H_2O concentrations during the synthesis of the n-type $TiO_2{}^m$ semiconductor also have an important influence on the behavior of the performance parameters of the DSSC (I_{SC}, V_{OC}, FF, and η%). By varying the concentration of the catalyst (HCl) during hydrolysis of the precursor, a greater variation in the short-circuit current J_{SC} is observed in the *I-V* curve of the DSSC, with a greater dispersion of the values of the performance parameters of the solar cells (I_{SC}, V_{OC}, FF, and η%).

On the contrary, by optimizing the H_2O concentration during the synthesis of the *n*-type $TiO_2{}^m$ semiconductor, in the analyzed DSSC, the values of the open-circuit voltage V_{OC} and fill factor (FF) are more uniform and less disperse than those for $TiO_2{}^m$ synthesized at different HCl concentrations. On average, the short-circuit currents J_{SC} and conversion efficiency η% of the cells whose synthesis of $TiO_2{}^m$ was optimized by adjusting the H_2O content surpass those optimized by adjusting only the HCl concentration. The highest conversion efficiency (η%) found in the DSSC reported in this study was 4.08%.

In summary, the performance parameters (I_{SC}, V_{OC}, FF, and η%) of DSSC were greatly influenced by the HCl and H_2O concentrations used during hydrolysis of the titanium isopropoxide precursor in the synthesis of the *n*-type $TiO_2{}^m$ semiconductor.

Data Availability

This research article is the result of the Ph.D. dissertation in Engineering and Applied Sciences of the student Sergio Velazquez Martínez carried out in the Research Institute of Basic and Applied Sciences of the Autonomous University of the State of Morelos, Mexico. The data of said results are available in the student's work log which is available in the aforementioned institute.

Conflicts of Interest

The authors declare that they have no conflicts of interest.

Acknowledgments

This study was performed with financial support from the Energy Sustainability Fund SENER-CONACYT-Mexico through project B-S-69369 (Bilateral project Mexico-England) and from DGAPA-PAPIIT through project IT101118. The authors thank M. Sc. Ma. Luisa Ramón García for her support in measuring and analyzing the X-ray diffraction patterns of the TiO_2 blocking and mesoporous films, Eng. Rogelio Moran Elvira for his support in the scanning electron microscopy measurements and Engs. A. Palafox and E. Luna for their technical assistance in the development of the transparent conductor of SnO_2: F.

References

[1] B. O'Regan and M. Grätzel, "A low-cost, high-efficiency solar cell based on dye-sensitized colloidal TiO_2 films," *Nature*, vol. 353, pp. 737–740, 1991.

[2] M. Pazoki, U. B. Cappel, E. M. J. Johansson, A. Hagfeldt, and G. Boschloo, "Characterization techniques for dye-sensitized solar cells," *Energy & Environmental Science*, vol. 10, no. 3, pp. 672–709, 2017.

[3] M. Ye, X. Wen, M. Wang et al., "Recent advances in dye-sensitized solar cells: from photoanodes, sensitizers and electrolytes to counter electrodes," *Materials Today*, vol. 18, no. 3, pp. 155–162, 2015.

[4] M. Grätzel, "The advent of mesoscopic injection solar cells," *Progress in Photovoltaics: Research and Applications*, vol. 14, no. 5, pp. 429–442, 2006.

[5] M. Grätzel, "Dye-sensitized solar cells," *Journal of Photochemistry and Photobiology C: Photochemistry Reviews*, vol. 4, no. 2, pp. 145–153, 2003.

[6] R. Govindaraj, N. Santhosh, M. Senthil Pandian, and P. Ramasamy, "Preparation of titanium dioxide nanorods/nanoparticles via one-step hydrothermal method and their influence as a photoanode material in nanocrystalline dye-sensitized solar cell," *Applied Surface Science*, vol. 449, pp. 166–173, 2018.

[7] M. Jalali, R. Siavash Moakhar, A. Kushwaha, G. K. L. Goh, N. Riahi-Noori, and S. K. Sadrnezhaad, "Enhanced dye loading-light harvesting TiO_2 photoanode with screen printed nanorod-nanoparticles assembly for highly efficient solar cell," *Electrochimica Acta*, vol. 169, pp. 395–401, 2015.

[8] V. Karthikeyan, S. Maniarasu, V. Manjunath, E. Ramasamy, and G. Veerappan, "Hydrothermally tailored anatase TiO_2 nanoplates with exposed {1 1 1} facets for highly efficient dye-sensitized solar cells," *Solar Energy*, vol. 147, pp. 202–208, 2017.

[9] Y. Cui, X. He, M. Zhu, and X. Li, "Preparation of anatase TiO_2 microspheres with high exposure (001) facets as the light-scattering layer for improving performance of dye-sensitized solar cells," *Journal of Alloys and Compounds*, vol. 694, pp. 568–573, 2017.

[10] S. Kathirvel, C. Su, Y.-J. Shiao, Y.-F. Lin, B.-R. Chen, and W.-R. Li, "Solvothermal synthesis of TiO_2 nanorods to enhance photovoltaic performance of dye-sensitized solar cells," *Solar Energy*, vol. 132, pp. 310–320, 2016.

[11] M. Gao, Y. Ma, L. Qi, J. Liang, Y. Si, and Q. Zhang, "Anatase TiO_2 nanocrystals via dihydroxy bis (ammonium lactato) titanium (IV) acidic hydrolysis and its performance in dye-sensitized solar cells," *Journal of Porous Materials*, vol. 25, no. 5, pp. 1499–1504, 2018.

[12] A. Hagfeldt, G. Boschloo, L. Sun, L. Kloo, and H. Pettersson, "Dye-sensitized solar cells," *Chemical Reviews*, vol. 110, no. 11, pp. 6595–6663, 2010.

[13] M. K. Nazeeruddin, E. Baranoff, and M. Grätzel, "Dye-sensitized solar cells: a brief overview," *Solar Energy*, vol. 85, no. 6, pp. 1172–1178, 2011.

[14] S. Sharma, B. Bulkesh Siwach, S. K. Ghoshal, and D. Mohan, "Dye sensitized solar cells: from genesis to recent drifts," *Renewable and Sustainable Energy Reviews*, vol. 70, pp. 529–537, 2017.

[15] M. Shakeel Ahmad, A. K. Pandey, and N. Abd Rahim, "Advancements in the development of TiO_2 photoanodes and its fabrication methods for dye sensitized solar cell (DSSC) applications. a review," *Renewable and Sustainable Energy Reviews*, vol. 77, pp. 89–108, 2017.

[16] J. Gong, J. Liang, and K. Sumathy, "Review on dye-sensitized solar cells (DSSCs): fundamental concepts and novel materials," *Renewable and Sustainable Energy Reviews*, vol. 16, no. 8, pp. 5848–5860, 2012.

[17] J. Gong, K. Sumathy, Q. Qiao, and Z. Zhou, "Review on dye-sensitized solar cells (DSSCs): advanced techniques and research trends," *Renewable and Sustainable Energy Reviews*, vol. 68, pp. 234–246, 2017.

[18] S. Mozaffari, M. R. Nateghi, and M. B. Zarandi, "An overview of the challenges in the commercialization of dye sensitized solar cells," *Renewable and Sustainable Energy Reviews*, vol. 71, pp. 675–686, 2017.

[19] P. P. Kumavat, P. Sonar, and D. S. Dalal, "An overview on basics of organic and dye sensitized solar cells, their mechanism and recent improvements," *Renewable and Sustainable Energy Reviews*, vol. 78, pp. 1262–1287, 2017.

[20] S. V. Umale, S. N. Tambat, V. Sudhakar, S. M. Sontakke, and K. Krishnamoorthy, "Fabrication, characterization and comparison of DSSC using anatase TiO_2 synthesized by various methods," *Advanced Powder Technology*, vol. 28, no. 11, pp. 2859–2864, 2017.

[21] G. Li, C. P. Richter, R. L. Milot et al., "Synergistic effect between anatase and rutile TiO_2 nanoparticles in dye-sensitized solar cells," *Dalton Transactions*, vol. 45, pp. 10078–10085, 2009.

[22] M. Grätzel, "Solar energy conversion by dye-sensitized photovoltaic cells," *Inorganic Chemistry*, vol. 44, no. 20, pp. 6841–6851, 2005.

[23] K. D. Benkstein, N. Kopidakis, J. van de Lagemaat, and A. J. Frank, "Influence of the percolation network geometry on electron transport in dye-sensitized titanium dioxide solar cells," *Journal of Physical Chemistry B*, vol. 107, no. 31, pp. 7759–7767, 2003.

[24] Y. T. Chung, M. M. Ba-Abbad, A. W. Mohammad, N. H. H. Hairom, and A. Benamor, "Synthesis of minimal-size ZnO nanoparticles through sol-gel method: taguchi design optimisation," *Materials and Design*, vol. 87, pp. 780–787, 2015.

[25] H. Tong, N. Enomoto, M. Inada, Y. Tanaka, and J. Hojo, "Synthesis of mesoporous TiO_2 spheres and aggregates by sol-gel method for dye-sensitized solar cells," *Materials Letters*, vol. 141, pp. 259–262, 2015.

[26] T. Sugimoto, X. Zhou, and A. Muramatsu, "Synthesis of uniform anatase TiO_2 nanoparticles by gel-sol method," *Journal of Colloid and Interface Science*, vol. 259, no. 1, pp. 43–52, 2003.

[27] F. Gu, S. F. Wang, M. K. Lü, G. J. Zhou, D. Xu, and D. R. Yuan, "Photoluminescence properties of SnO_2Nanoparticles synthesized by sol–gel method," *Journal of Physical Chemistry B*, vol. 108, no. 24, pp. 8119–8123, 2004.

[28] E. Lifshitz, I. Dag, I. Litvin et al., "Optical properties of CdSe nanoparticle films prepared by chemical deposition and sol-gel methods," *Chemical Physics Letters*, vol. 288, no. 2–4, pp. 188–196, 1998.

[29] B. Gersten, "Solvothermal synthesis of nanoparticles," *Chemfiles*, vol. 5, pp. 11-12, 2005.

[30] J. Archana, M. Navaneethan, and Y. Hayakawa, "Solvothermal growth of high surface area mesoporous anatase TiO_2 nanospheres and investigation of dye-sensitized solar cell properties," *Journal of Power Sources*, vol. 242, pp. 803–810, 2013.

[31] F. Sauvage, D. Chen, P Comte et al., "Dye-sensitized solar cells employing a single film of mesoporous TiO_2 beads achieve

power conversion efficiencies over 10%," *ACS Nano*, vol. 4, no. 8, pp. 4420–4425, 2010.

[32] D. Chen, F. Huang, Y.-B. Cheng, and R. A. Caruso, "Mesoporous anatase TiO_2beads with high surface areas and controllable pore sizes: a superior candidate for high-performance dye-sensitized solar cells," *Advanced Materials*, vol. 21, no. 21, pp. 2206–2210, 2009.

[33] J. Archana, S. Harish, M. Sabarinathan et al., "Highly efficient dye-sensitized solar cell performance from template derived high surface area mesoporous TiO_2 nanospheres," *RSC Advances*, vol. 6, no. 72, pp. 68092–68099, 2016.

[34] Y. Rui, L. Wang, J. Zhao et al., "Template-free synthesis of hierarchical TiO_2 hollow microspheres as scattering layer for dye-sensitized solar cells," *Applied Surface Science*, vol. 369, pp. 170–177, 2016.

[35] Z.-Q. Li, Y.-P. Que, L.-E. Mo et al., "One-pot synthesis of mesoporous TiO_2 micropheres and its application for high-efficiency dye-sensitized solar cells," *ACS Applied Materials & Interfaces*, vol. 7, no. 20, pp. 10928–10934, 2015.

[36] A. E. J. González and S. G. Santiago, "Structural and opto-electronic characterization of TiO_2 films prepared using the sol-gel technique," *Semiconductor Science and Technology*, vol. 22, no. 7, pp. 709–716, 2007.

[37] C.-C. Wang and J. Y. Ying, "Sol-gel synthesis and hydrothermal processing of anatase and rutile titania nanocrystals," *Chemistry of Materials*, vol. 11, no. 11, pp. 3113–3120, 1999.

[38] B. A. Morales, O. Novaro, T. López, E. Sánchez, and R. Gómez, "Effect of hydrolysis catalyst on the Ti deficiency and crystallite size of sol-gel-TiO_2 crystalline phases," *Journal of Materials Research*, vol. 10, no. 11, pp. 2788–2796, 1995.

[39] C. J. Brinker and G. W. Scherer, *Sol-Gel Science: The Physics and Chemistry of Sol-Gel Processing*, Academic Press INC, Cambridge, MA, USA, 1990.

[40] T. Tesfamichael, G. Will, J. Bell, K. Prince, and N. Dytlewski, "Characterization of a commercial dye-sensitised titania solar cell electrode," *Solar Energy Materials and Solar Cells*, vol. 76, no. 1, pp. 25–35, 2003.

[41] J. Tauc, "Absorption edge and internal electric fields in amorphous semiconductors," *Materials Research Bulletin*, vol. 5, no. 8, pp. 721–729, 1970.

[42] H.-J. Kim, J.-D. Jeon, and S.-Y. Kwak, "Highly dispersed mesoporous TiO_2 spheres via acid treatment and its application for dye-sensitized solar cells," *Powder Technology*, vol. 243, pp. 130–138, 2013.

[43] L. B. McCusker, F. Liebau, and G. Engelhardt, "Nomenclature of structural and compositional characteristics of ordered microporous and mesoporous materials with inorganic hosts," *Microporous and Mesoporous Materials*, vol. 58, no. 1, pp. 3–13, 2003.

[44] N. Laidani, R. Bartali, G. Gottardi, M. Anderle, and P. Cheyssac, "Optical absorption parameters of amorphous carbon films from Forouhi–Bloomer and Tauc–Lorentz models: a comparative study," *Journal of Physics: Condensed Matter*, vol. 20, no. 1, article 015216, 2008.

[45] J. Du, J. Zhang, and D. J. Kang, "Controlled synthesis of anatase TiO_2 nano-octahedra and nanospheres: shape-dependent effects on the optical and electrochemical properties," *CrystEngComm*, vol. 13, no. 12, p. 4270, 2011.

[46] M. A. Sánchez-García, X. Bokhimi, A. Maldonado-Álvarez, and A. E. Jiménez-González, "Effect of anatase synthesis on the performance of dye-sensitized solar cells," *Nanoscale Research Letters*, vol. 10, no. 1, p. 306, 2015.

[47] K. S. Swathy, P. A. Abraham, N. R. Panicker, N. C. Pramanik, and K. S. Jacob, "Nanostructured anatase titania spheres as light scattering layer in dye-sensitized solar cells," *Procedia Technology*, vol. 24, pp. 767–773, 2016.

[48] C. Dwivedi, V. Duttaa, A. K. Chandiranb, V. Chandiran, M. K. Nazeeruddin, and M. Grätzel, "Anatase TiO_2 hollow microspheres fabricated by continuous spray pyrolysis as a scattering layer in dye-sensitised solar cells," *Energy Procedia*, vol. 33, pp. 223–227, 2013.

[49] X. Miao, K. Pan, Y. Liao et al., "Controlled synthesis of mesoporous anatase TiO_2 microspheres as a scattering layer to enhance the photoelectrical conversion efficiency," *Journal of Materials Chemistry A*, vol. 1, no. 34, p. 9853, 2013.

[50] M.-J. Jeng, Y.-L. Wung, L.-B. Chang, and L. Chow, "Dye-sensitized solar cells with anatase TiO_2 nanorods prepared by hydrothermal method," *International Journal of Photoenergy*, vol. 2013, Article ID 563897, 9 pages, 2013.